# 2-D Asymmetric Induced Phase Modulation: Spatial and Spatio-Temporal Aspects

N. Goutev, A. Dreischuh, S. Baluschev, and S. Dinev

*Abstract*— **A multidimensional generalization of the Fresnel-Kirchhoff theory for analyzing the far-field pattern of a probe beam/pulse, passing trough a thin nonlinear medium is developed. The experimental results obtained agree qualitatively with the theoretical predictions. It is shown that the asymmetric induced-phase modulation offers the possibility for a simultaneous shaping and shortening of probe pulses.**

## I. Introduction

THE SELF-PHASE MODULATION (SPM) and induced-phase modulation (IPM, XPM) originate in the (self)induced refractive index change in the nonlinear media. Self-bending of a nonuniform laser beam due to a nonuniform medium refractive index change [1] is observed with beams incident on nonlinear media at certain angles [2]. In a later work, a self-deflection of an asymmetrical (spatially filtered) beam in a resonant nonlinear medium [3] and bulk Kerr material [4] are observed experimentally in agreement with the theory. The IPM, however, makes the physical picture more complicated because of the possible mutual temporal delay and/or the eventual axial offset between the beams/pulses. In the spatial domain, an induced focusing of optical beams in an off-axis geometry, occurring in self-defocusing nonlinear media is proposed [5] and confirmed experimentally [6], [7]. It is shown theoretically, that the conditions, under which induced beam-deflection can occur, depend also on the interaction geometry and induced focusing may occur under self-focusing conditions too [8], [14]. The intensity-dependent self-deflection, combined with a far-field spatial filtering could be used for picosecond laser-pulse shortening [4]. This result indicates, that the IPM should be analyzed carefully in more than one transverse dimension.

The aim of this paper is to show that the 2-D spatial or spatio-temporal experimental-data acquisition (theoretical modeling, respectively) may lead to results quite different from those obtained in a 1-D experiment (theory) in space or time separately. The theoretical model developed and the experiment performed strongly support this statement. The angular-spectral intensity distribution of a beam/pulse with an asymmetric induced phase modulation (AIPM) should be considered as a source of potential experimental inaccuracies. On the other hand, a simple far-field spatial filtering should lead to a simultaneous pulse shaping and shortening of the transmitted signal.

Manuscript received October 31, 1994; revised June 30, 1995. This work was done with the financial support of the National Science Found, Bulgaria, under a contract #MU-TT-1/1991.

The authors are with the Department of Physics, Sofia University, 1126 Sofia, Bulgaria.

IEEE Log Number 9415435.

## II. Theoretical Model

In order to describe the evolution of AIPM beams/pulses in a dispersive linear medium we develop a model, which is a multidimensional generalization of the Fresnel–Kirchhoff theory [9]. In an infinite isotropic linear medium, the optical field amplitude could be expressed as a superposition of plane waves [9]

$$E(x,y,z,t)=\int_{-\infty}^{+\infty}\int_{-\infty}^{+\infty}\int_{-\infty}^{+\infty}E(k_x,k_y,\omega)\cdot\exp\{i(kr-\omega t)\}\,dk_x\,dk_y\,d\omega. \quad (1)$$

where $k=(k_x, k_y, k_z)$ is the wave-vector, $\omega$ is the angular frequency and $k_x, k_y, k_z, \omega$ satisfy the dispersive equation

$$k_z=[\beta^2(\omega)-k_x^2-k_y^2]^{1/2} \quad (2a)$$

and

$$\beta(\omega)=n(\omega)(\omega/c). \quad (2b)$$

In (2b), $\beta(\omega)$ is the wave-number and $n(\omega)$ is the medium linear refractive index. The function $E(k_x, k_y, \omega)$ represents the initial amplitude angular-frequency field-distribution and could be obtained by a Fourier-transformation of $E(x, y, z=0, t)$.

Let us consider an optical field with a narrow angular-frequency spectrum localized around $(k_x, k_y, \omega)=(0, 0, \omega_0)$. In this case, neglecting the third and higher order terms, the Taylor-series expansion of the dispersive equation (2a) yields:

$$k_z=\beta_0+\beta_0^{(1)}\Delta\omega+[\beta_0^{(2)}\Delta\omega^2]/2-[k_x^2+k_y^2]/(2\beta_0). \quad (3)$$

where

$$\beta_0^{(n)}=\beta^{(n)}(\omega_0), \qquad n=0,1,2 \quad (4)$$

are the $n$th derivatives of the wave-number at the center frequency $\omega_0$. Substituting the reduced dispersive equation (3) in (1) one can obtain

$$E(x,y,z,t)=\exp\{i(\beta_0 z-\omega_0 t)\}\int_{-\infty}^{+\infty}\int_{-\infty}^{+\infty}\int_{-\infty}^{+\infty}\cdot E(k_x,k_y,\omega_0+\Delta\omega)\cdot\exp\{i[\beta_0^{(2)}\Delta\omega^2]/2-i[k_x^2+k_y^2]/(2\beta_0 z)\}\cdot\exp\{i(k_x x+k_y y-\Delta\omega\tau)\}\,dk_x\,dk_y\,d\Delta\omega, \quad (5)$$

where $\tau = t - \beta_0^{(1)} z$ is the temporal coordinate in a coordinate frame, moving at a group velocity $V_{gr} = 1/\beta_0^{(1)}$. It is convenient to introduce the slowly-varying amplitude (SVA) $\tilde{E}(x, y, z, \tau)$:

$$E(x, y, z, t) = \tilde{E}(x, y, z, \tau) \exp\{i(\beta_0 z - \omega_0 t)\}. \quad (6)$$

Rewriting (5) in terms of $\tilde{E}(x, y, z, \tau)$ and it's angular-frequency spectrum $\tilde{E}(k_x, k_y, \Delta\omega)$ one obtains the result

$$\tilde{E}(x, y, z, \tau) = \int_{-\infty}^{+\infty}\int_{-\infty}^{+\infty}\int_{-\infty}^{+\infty} \tilde{E}(x_0, y_0, 0, \tau_0) \cdot W(x_0 - x, y_0 - y, \tau_0 - \tau, z)\, dx_0\, dy_0\, d\tau_0, \quad (7)$$

where

$$W(x_0 - x, y_0 - y, \tau_0 - \tau, z) = (2\pi)^{-3}[2\pi/(-iz\beta_0^{(2)})]^{1/2}[2\pi\beta_0/(iz)] \cdot \exp\left\{\frac{i\beta_o}{2z}[(\tau_0 - \tau)^2/(-\beta_0^{(2)}/\beta_0) + (x_0 - x)^2 + (y_0 - y)^2]\right\} \quad (8)$$

can be referred to as a linear dispersive-medium transmission function. Equation (7) should be considered as a multidimensional generalization of the Huygens–Fresnel integral [9] for optical fields under SVA approximation. In the rest of this section we analyze the particular case of a Fraunhofer diffraction. Let us assume that in the input plane $z = 0$ the optical field is localized in a spatial region of a transverse dimension (2a) and in a temporal region of an extent $2\Delta\tau$. In this case the infinite integration space could be restricted to an integration within the intervals $[-a, a] \times [-a, a] \times [-\Delta\tau, \Delta\tau]$. According to (7), for all the points of coordinates $(x, y, z, \tau)$ which simultaneously satisfy the conditions $x \gg a$, $y \gg a$, $\tau \gg \Delta\tau$, the slowly-varying field amplitude $\tilde{E}$ has the form:

$$\tilde{E}(x, y, z, \tau) = C(z) \exp\{i(\beta/2z)[(\tau_0^2/(-\beta_0\beta_0^{(2)}) + x_0^2 + y_0^2]\} \cdot \int_{-a}^{+a}\int_{-a}^{+a}\int_{-\Delta\tau}^{+\Delta\tau} \tilde{E}(x_0, y_0, 0, \tau_0) \cdot \exp\{-i(\beta_0/z)[\tau_0\tau/(-\beta_0\beta_0^{(2)}) + x_0 x + y_0 y]\} dx_0\, dy_0\, d\tau_0, \quad (9)$$

where

$$C(z) = (2\pi)^{-3}[2\pi/(-iz\beta_0^{(2)})]^{1/2}[2\pi\beta_0/(iz)].$$

Because of the assumed spatio-temporal localization of the optical field in the plane $z = 0$, the limited integration space could be expanded to infinity. This form of (9) is a generalization of the Fraunhofer diffraction integral [9].

Further, we will discuss two particular cases of a Fraunhofer diffraction involving a monochromatic input optical field (2-D spatial configuration) and an optical field of a translation symmetry (2-D spatio-temporal configuration).

### A. 2-D Spatial Configuration

In the case of a monochromatic input optical field, the SVA field-amplitude does not depend on time. Accounting for this fact in (9), at a second plane with a nonzero $z$ coordinate, the corresponding field-distribution has the form

$$\tilde{E}(x, y, z) = (2\pi)^{-2}[2\pi\beta_0/(iz)] \exp\{[i\beta_0/(2z)][x_0^2 + y_0^2]\} \cdot \int_{-\infty}^{+\infty}\int_{-\infty}^{+\infty} \tilde{E}(x_0, y_0, 0) \cdot \exp\{[-i\beta_0/z][x_0 x + y_0 y]\}\, dx_0\, dy_0. \quad (10)$$

which, in the angular domain, is related to the distribution

$$\tilde{E}(k_x, k_y) = (2\pi)^{-2}\int_{-\infty}^{+\infty}\int_{-\infty}^{+\infty} \tilde{E}(x_0, y_0, 0) \cdot \exp\{-i(k_x x_0 + k_y y_0\}\, dx_0\, dy_0. \quad (11)$$

### B. 2-D Spatio-Temporal Configuration

At a translation symmetry of the input optical field in $x$-direction, the SVA field-amplitude does not depend on the $x$-coordinate. At a second plane located at $z \neq 0$,

$$\tilde{E}(y, z, \tau) = (2\pi\beta/(iz))[\beta_0/(-\beta_0^{(2)})]^{1/2} \cdot \exp\{i\beta_0/(2z)[(\tau_0^2/(-\beta_0\beta_0^{(2)}) + y_0^2]\} \cdot \int_{-\infty}^{+\infty}\int_{-\infty}^{+\infty} \tilde{E}(y_0, 0, \tau_0) \cdot \exp\{-i\beta_0/z[\tau_0\tau/(-\beta_0\beta_0^{(2)}) + y_0 y]\} dy_0\, d\tau_0. \quad (12)$$

which is related to the angular-frequency field distribution:

$$\tilde{E}(\Delta\omega, k_y) = (2\pi)^{-2}\int_{-\infty}^{+\infty}\int_{-\infty}^{+\infty} \tilde{E}(y_0, \tau_0, 0) \cdot \exp\{-i[k_y y_0 - \Delta\omega\tau_0]\}\, dy_0\, d\tau_0. \quad (13)$$

## III. 2-D Asymmetric Induced-Phase Modulation

### A. Spatial Aspects

Let us consider the following interaction configuration (Fig. 1). Two laser beams (a pump and a weak non-self-acting probe one) enter a nonlinear medium of thickness l with an initial off-axis separation $\Delta y$. Both beams are assumed to be mutually incoherent, Gaussian and are focused to equal beam waists. The nonlinear medium is assumed to exhibit a third order nonlinearity with a local and instantaneous response. The far-field pattern could be observed on a screen, placed at a distance $L$ behind the exit of the nonlinear medium. If the medium length $l$ is much less than both the nonlinear and the diffraction lengths, the beam shapes remain nearly constant inside the nonlinear medium [10]. Therefore, at the entrance face and within the medium of length $l$, the square of the pump ($E_p$) and probe-field ($E_s$) amplitudes could be described by:

$$|E_p|^2 = |E_p^0|^2 \exp\{-2r_1^2/a^2\} \quad (14a)$$

$$|E_s|^2 = |E_s^0|^2 \exp\{-2r^2/a^2\}, \quad (14b)$$

where $r_1^2 = (y - \Delta y)^2 + x^2$ and $r^2 = y^2 + x^2$. Because of its low intensity, the probe field does not cause nonlinear

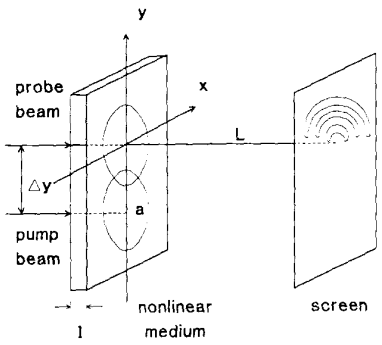


Fig. 1. Analyzed interaction configuration.

effects itself. The probe beam experiences an asymmetric phase modulation

$$\Delta\phi_s = \frac{2\pi}{\lambda_s} l \Delta n_s. \tag{15a}$$

only as a result of the refractive-index correction

$$\Delta n_s = 2n_2^{\mathrm{IPM}} |E_p^0|^2 \exp\{-2r_1^2/a^2\} \tag{15b}$$

induced by the pump. In (15) $n_2^{\mathrm{IPM}}(\lambda_s;\lambda_p)$ is the nonlinear refractive index of the medium at the probe wavelength $\lambda_s$ and may have a resonance character versus $\lambda_p$. At the exit of the medium the signal field-amplitude could be written as

$$E_s = E_s^0 \exp\{-2r^2/a^2\} \exp\{i\Delta\phi_s\}. \tag{16}$$

The 2-D angular probe beam field distribution (13b) could be obtained by a Fourier transformation of (16).

At this point it is convenient to introduce the parameter $N$, defined as the maximum phase shift $\Delta\phi_s^{\max}$ divided by $(2\pi)$. Physically, $N$ is the number of the far-field interference fringes of the probe beam at an on-axis interaction. The dimensionless coordinates $\overline{x_0}$, $\overline{y_0}$, $\overline{r_0}$, $\overline{\Delta y}$, and $\overline{r_1}$ used in the numerical simulations corresponded to the respective spatial coordinates normalized to the beam radii (assumed to be equal). Similarly, the dimensionless angular coordinates $\overline{\alpha_x}$, $\overline{\alpha_y}$ are introduced with a normalization to the angle of diffraction $\alpha_{\mathrm{diff}}$

$$\overline{\alpha_x} = \alpha_x/\alpha_{\mathrm{diff}} = k_x a/(2\pi) \tag{17a}$$

$$\overline{\alpha_y} = \alpha_y/\alpha_{\mathrm{diff}} = k_y a/(2\pi). \tag{17b}$$

In the above notations, the angular probe beam distribution (11) takes the form

$$\tilde{E}(\overline{\alpha_x},\overline{\alpha_y}) = \int_{-\infty}^{+\infty}\int_{-\infty}^{+\infty} \tilde{E}(x_0,y_0) \cdot \exp\{-i2\pi(\overline{\alpha_x}\overline{x_0} + \overline{\alpha_y}\overline{y_0})\}\, d\overline{x}\, d\overline{y}. \tag{17c}$$

where

$$\tilde{E}(\overline{x}_0,\overline{y}_0) = E_s^0 \exp\{-\overline{r}_0^2\} \exp\{i\Delta\phi_s\}, \tag{17d}$$

$$\Delta\phi_s = 2\pi N \exp\{-2\overline{r}_1^2\}, \tag{17e}$$

and could be evaluated by a 2-D Fourier-transformation.

The typical 2-D far-field angular distributions of the probe beam obtained numerically are shown on Fig. 2(a)–(c) at $N =$ 3.5. Fig. 2(a) corresponds to $\Delta y_0 = 0$ (i.e., on-axis beams). The number of interference fringes is equal to the integer part of $N$. Fig. 2(b) and (c) correspond to $\Delta y_0/a = 0.4$ and $\Delta y_0/a = 0.8$, respectively. The obvious asymmetry of $I_s(\overline{\alpha_x}, \overline{\alpha_y})$ is a result of the probe beam AIPM. The interference fringes evolve in arcs. At a relatively small offset $\Delta y_0$, the number of arcs is equal to the integer part of $N$. At higher off-axis separations ($\Delta y_0/a = 0.4$) some of the arcs are of reduced contrast [Fig. 2(b)]. Increasing the initial spatial beam separation, the AIPM decreases due to the decreased effective beam-overlapping. The probe beam wing-oscillations become weaker and the central part of the beam grows [Fig. 2(c)] approaching the undisturbed Gaussian spatial distribution. It is essential to note, that the off-axial separation $\Delta y_0$ breaks the radial symmetry of the problem and the AIPM leads to a modulation in the $(\overline{\alpha_x}, \overline{\alpha_y})$-space.

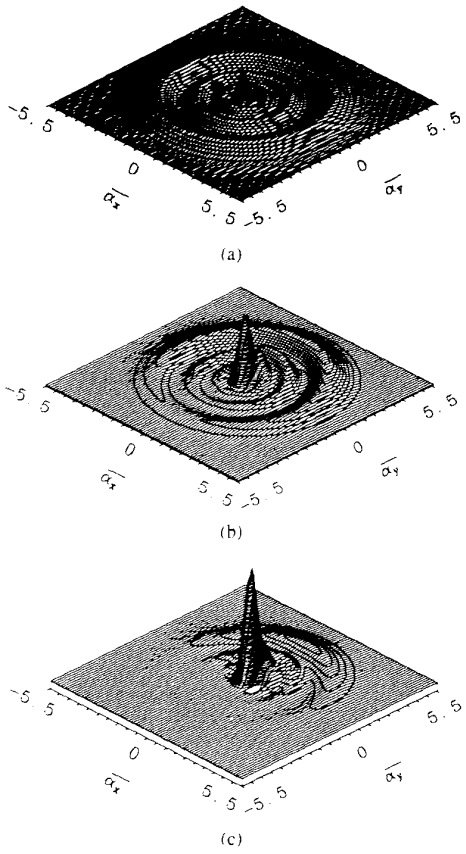


Fig. 2. (a) Two-dimensional probe beam far-field energy distribution at on-axis beams, (b) $y_0/a = 0.4$, and (c) $y_0/a = 0.8$, $N = 3.5$.

Qualitatively, the results presented on Fig. 2(a)–(c) can be explained in the following way. Each part of the phase-modulated probe beam could be considered as a sequential plane-wave propagating at an angle

$$\alpha = \Delta_{-}o/\beta$$

with respect to the initial axis of the probe beam. These sequential waves interfere and minima (maxima, respectively)

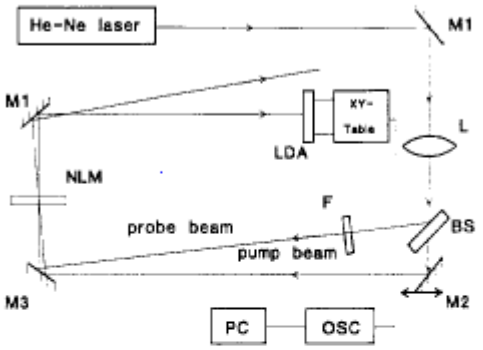


Fig. 3. Experimental setup for observing a 2-D spatial optical wave-breaking ($M1$–$M4$—mirrors; $L$—lens; $BS$—beam-splitter; $F$—filter; $NLM$—thin nonlinear medium; $LDA$—linear diode array).

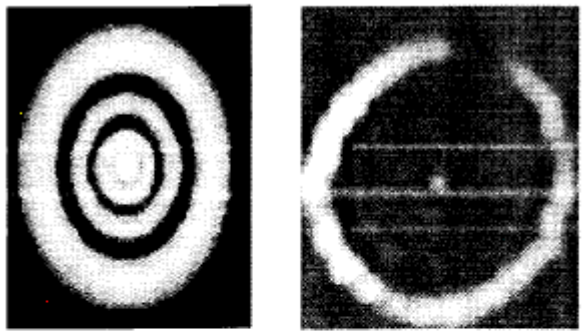

(a) (b)

Fig. 4. (a) Topology of the theoretically obtained 2-D probe-beam far-field pattern at on-axis beams [see Fig. 2(a)] and (b) experimentally obtained result.

should be observed. If both beams are on-axially aligned, the probe-beam phase distribution $\Delta\phi_s$ is symmetrical. The interference pattern should consist of maxima in the form of coaxial rings [Fig. 2(a)]. At an initial pump-to-probe axial offset the phase distribution $\Delta\phi_s$ is asymmetrical. The sequential waves from the less phase modulated probe-beam wing, which contribute to the interference maximum, are weaker. In this section of the probe-beam pattern, the interference maxima are of reduced intensity [Fig. 2(b)] and some interference fringes break in arcs [Fig. 2(c)].

### *B. Experimental Results*

The experimental setup is sketched on Fig. 3. Briefly, the output of a single-mode He–Ne laser ($P_{\max} = 50$ mW) was gently focused and split into two parts with a variable pump-to-probe intensity ratio of at least 100. The pump channel comprised translation stage in order to adjust the beam off-axis distance. Both beams ($P_{\text{pump}}^{\max} \leq 25$ mW) entered a 1-mm quartz quivette filled with ethanol, slightly dyed with Nile Blue (Lambdachrome). The quivette was mounted horizontally in order to prevent liquid's convection. This combination allowed a strong (up to $\overline{\alpha_y} \simeq 15$) thermal self-defocusing on the pump beam to be observed without a probe-beam self-action. The 2-D spatial data acquisition was performed by translating a 1024 element linear diode array (RETICON RL-1024G) connected with a digital storage oscilloscope and a PC-compatible computer. Let us define an effective laser beam as a beam, which evolves in- and outside a medium with a local nonlinear response in the same way, as compared to the beam in the present (nonlocal) experiment. We measured the number of rings and the outer ring diameter of the pump beam versus pump power. The perfect linearity of these dependencies is indicative for the absence of saturation in the SPM of the pump and, therefore, of the probe-beam AIPM. Following the approach from [11], [12], from the nonlinear deflection angle $\theta^{NL} = 6.1$ mrad, experimentally obtained at $N = 5$, we deduced an effective pump/probe beam radius $a = 500$ $\mu$m and an effective nonlinear refractive index $n_2 = -1.1.10^{-3}$ cm$^2$/W (i.e., $\Delta n = n_2 I = 3.10^{-3}$ and $(\overline{\alpha_y})_{\max} \simeq 15$). In order to achieve accurate numerical results with a two-dimensional Fourier transformation of the modulated probe beam over 256 $\times$ 256 grid pints, we chose $n_2$ to be 1.4 times lower than the experimental value (i.e., $N = 3.5$). This scaling results in a 1.4 times reduction of the numerically obtained nonlinear deflection angle ($\theta^{NL} = 4.4$ mrad and $(\overline{\alpha_y})_{\max} \simeq 11$), but does not affect the confidence of the numerical presented results.

Figs. 4(a), 5(a), and 6(a) are gray-scale images of the theoretical results shown on Fig. 2. The circular symmetry of the far-field pattern in the case of on-axis beams [Fig. 4(a)], as well as the probe-beam spatial oscillations due to the AIPM [Figs. 5(a), 6(a)] are clearly seen. Fig. 4(b) shows the experimental far-field probe-beam pattern obtained in an on-axis geometry and at a quivette input pump power of 23 mW. As expected, the picture is nearly circularly symmetric. Because of the limited dynamic range of the linear diode array only the beam center and the outer fringe are clearly displayed, but, in fact, the number of fringes is five. A small ellipticity is induced by the nonequal heat-conduction conditions within the quivette. Fig. 5(b) plots the far-field probe-beam pattern at an initial 150 $\mu$m separation of the 500 $\mu$m-sized pump- and probe beams (i.e., $\Delta y/a \approx 0.32$). Qualitatively, the experimental picture [Fig. 5(b)] is similar to the theoretical prediction at $\Delta y/a = 0.4$ [Fig. 5(a)]. The higher visibility of the probe-beam arcs (i.e., of the spatial oscillations due to the AIPM) could be explained by their comparable local peak energy densities. Fig. 6(b) plots the same experimental picture at $\Delta y/a = 0.5$. Qualitatively, it is comparable to the predicted far-field probe beam pattern at $\Delta y/a = 0.8$ [Fig. 6(a)]. The enhanced off-axis distance and the reduced beam overlapping lead to a weakly distorted central part of the probe beam dominating the oscillatory wings. Comparing the 2-D theoretical results [Figs. 4(a), 5(a), and 6(a)) with the experimental data obtained (Figs. 4(b), 5(b), and 6(b)] we found a good qualitative agreement. Quantitative comparison, however, is difficult to be done due to the complicated two-dimensional character of the interaction, limited dynamic range of the diode array, etc. The main problem seems to be that the thermal nonlinearity is nonlocal, whereas a localized nonlinearity is assumed in the model developed (see Section II-A). In principle, the nonlocality of the thermal experiment can be overcome by using a larger beam size at higher input powers.

In view of the good qualitative agreement between the theoretical predictions and the experimental results we believe that the 2-D model developed in Section II describes adequately

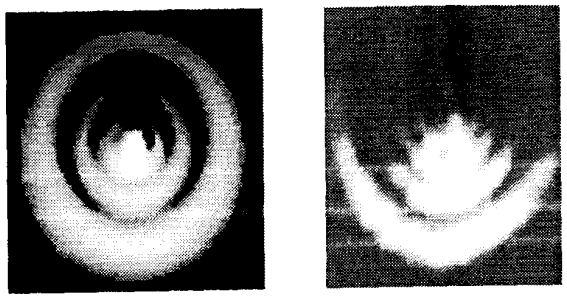

(a) (b)

Fig. 5. (a) Topology of the theoretically obtained 2-D probe-beam far-field pattern at $y_o/a = 0.4$ [see Fig. 2(b)] and (b) experimental result at $y_o/a = 0.32$.

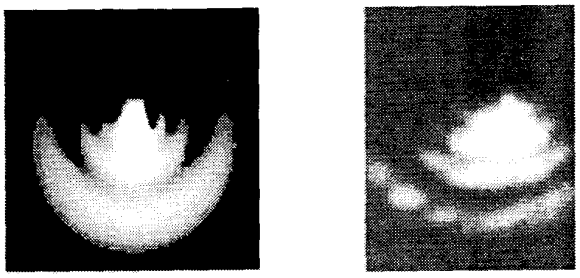

(a) (b)

Fig. 6. (a) Topology of the theoretically obtained 2-D probe-beam far-field pattern at $y_o/a = 0.8$ [see Fig. 2(c)] and (b) experimental result at $y_o/a = 0.5$.

the AIPM in a nonlinear medium of local and instantaneous nonlinearity.

### C. Spatio-Temporal Aspects

Further, we analyze in more details the situation depicted on Fig. 7. Two laser beams/pulses focused with a cylindrical lens into a spot of a high ellipticity enter a cubic nonlinear medium with a mutual temporal delay $\Delta\tau$ and/or an initial off-axis separation $\Delta y$. Because of the translation symmetry, the evolution of the intensity distribution in one spatial dimension could be neglected. Under the assumptions made in Section III-A, the square of the pump and probe field amplitudes are considered to be of the form

$$|E_p|^2 = |E_p^0|^2 \exp\{-2y_1^2/a^2\} \exp\{-2\tau_1^2/\Delta t^2\}, \quad (18a)$$

$$|E_s|^2 = |E_s^0|^2 \exp\{-2y^2/a^2\} \exp\{-2\tau^2/\Delta t^2\}. \quad (18b)$$

where $\Delta t$ are the pulse durations (assumed to be equal), $y_1 = y - \Delta y, \tau_1 = \tau - \Delta\tau$. The probe field amplitude at the exit of the nonlinear medium is described by

$$E_s = E_s^0 \exp\{-y^2/a^2\} \exp\{-\tau^2/\Delta t^2\} \exp\{i\Delta\phi_s\}. \quad (18c)$$

where

$$\Delta\phi_s = (2\pi/\lambda_s)1\{2n_2^{\mathrm{IPM}}|E_p|^2\} \quad (18d)$$

is the nonlinear part of the probe-beam phase profile induced by the pump. The angular-frequency distribution of the

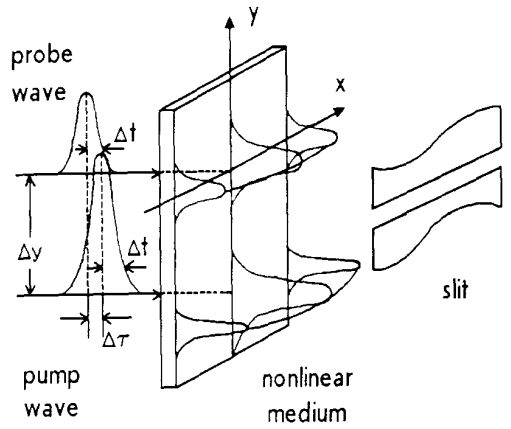


Fig. 7. Interaction configuration with a simultaneous spatio-temporal beam/pulse offset.

beam/pulse could be obtained by performing a 2-D Fourier transformation of the form given by (13).

Introducing the dimensionless coordinates and angles as done in Section III-A, the normalized probe-pulse frequency $\overline{\Delta\omega}$ should be defined as $\overline{\Delta\omega} = \Delta\omega/(2\pi/\Delta t)$. The spatio-temporal beam/pulse offset $\Delta$ could be introduced as follows

$$\Delta^2 = \overline{\Delta y}^2 + \overline{\Delta\tau}^2. \quad (19)$$

where the spatial offset $\overline{\Delta y}$ and the temporal delay $\overline{\Delta\tau}$ are normalized to the beam radius a and the pulse duration $\Delta t$, respectively. A coordinate system rotation at an angle

$$\upsilon = \operatorname{arctg}(\overline{\Delta\tau}/\overline{\Delta y}) \quad (20)$$

should lead to a new coordinate system $(\xi, \eta)$ with an $\eta$-axis crossing both the beam/pulse centers. The new coordinates $(\xi, \eta)$ correspond to complementary frequency coordinates $(\nu_\xi, \nu_\eta)$. The transition from the normalized frequency space $(\overline{\alpha_y}, \overline{\Delta\omega})$ to the frequency space $(\nu_\xi, \nu_\eta)$ should be carried out with a rotation at an angle $\upsilon$ of the form

$$\overline{\alpha_y} = \nu_\xi \sin(\upsilon) + \nu_\eta \cos(\psi) \quad (21a)$$

$$\overline{\Delta\omega} = \nu_\xi \cos(\upsilon) - \nu_\eta \sin(\psi). \quad (21b)$$

The reason to perform this procedure is that in the Fourier domain the probe wave amplitude $E_s(\nu_\xi, \nu_\eta)$ could be written in a form, analogous to that given by (17). Therefore, the numerical results [Figs. 4(a), 5(a), and 6(a)] are also applicable in the case of a simultaneous initial spatio-temporal beam/pulse offset.

Let us consider ones again the typical asymmetric far-field probe beam/pulse formation (Fig. 8), analogous, with regard to the above remarks, to the 2-D far-field spatial probe-beam pattern from Fig. 2(c). The angular-spectral characteristics of an AIPM beam/pulse are clearly expressed. The pattern consists mainly of components, satisfying the equation

$$\alpha_y^2/\alpha_{\mathrm{diff}}^2 + (\Delta\omega)^2/(2\pi/\Delta t)^2 = \Delta_i^2, \quad (22)$$

where $\Delta_i$ are parameters depending on the AIPM magnitude. The different frequency components have their maxima at different angles. In the case of ultrashort (broad bandwidth)

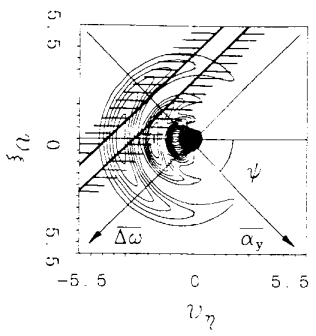


Fig. 8. Schema of the far-field spatial filtering by a slit.

pulses, this can lead to the formation of rings/arcs of different "colors" in the far-field. Let us suppose, that the probe wave is to be analyzed with spectral apparatus, e.g., a monochromator. The entrance slit will transmit only a part of the beam/pulse. At one and the same angular-frequency distribution different slit positions will result in different spectra recorded. Hence, the AIPM should be considered as a potential source of experimental inaccuracies.

A far-field spatial filtering of this kind can be useful if a simultaneous pulse shortening and shaping of the probe wave transmitted is desired [10]. Due to the higher local intensity it is naturally to expect, that the optical wavefront distortions of the probe wave would be most pronounced near the central part of the pump beam/pulse. In the leading and trailing wings of the pump pulse the number of the probe-beam interference rings/arcs and their radii would be reduced. A slit placed in the far field would transmit only this part of the probe wave, which would be more (or approximately equal) deflected compared to the offset of the slit with respect to the probe beam axis (Fig. 8). At temporally synchronized pump and probe pulses and a nonzero radial beam offset the slit would transmit a single pulse or pairs of pulses. Their durations should be reduced as compared to that of the incoming probe pulse. An eventual initial temporal delay combined with an initial beam offset (in space) should offer much wider possibilities for a simultaneous pulse shaping and shortening [10]. Quantitative comparison of experimental and numerical results on simultaneous probe-pulse shaping and shortening in the nanosecond time-scale will be published separately.

## IV. Conclusion

In this paper, we analyzed the 2-D asymmetric induced-phase modulation (AIPM) of a probe beam/pulse. A multidimensional generalization of the Fresnel–Kirchhoff theory was developed for analyzing the 2-D probe beam far-field pattern. It was shown that the physical picture of the AIPM should be analyzed at least in two dimensions. A good qualitative agreement was found between the theoretically predicted beam/pulse patterns and the experimentally obtained ones. It was shown, that the AIPM should be considered as a potential source of experimental inaccuracies but it offers the possibility a simultaneous pulse-shaping and shortening to be performed.

## References

[1] A. A. Kaplan, "Bending of trajectories of asymmetrical light beams in nonlinear media," *JETP Lett.*, vol. 9, pp. 3–7, 1969 (vol. 9, pp. 58–62, 1969, in Russian).
[2] B. M. Borodin and A. Kamuz, "Observation of self-bending of a nonuniform intense laser beam in an NaCl crystal," *JETP Lett.*, vol. 9, pp. 351–354, 1969 (vol. 9, pp. 577–580, 1969, in Russian).
[3] G. Swartzlander, Jr., H. Yiu, and A. Kaplan, "Continuous-wave self-deflection effect in sodium vapor," *J. Opt. Soc. Am.*, vol. B-6, pp. 1317–1325, 1989.
[4] A. Barthelemy, C. Froehly, S. Maneuf, and F. Reynaud, "Experimental observation of beam's self-deflection appearing with two-dimensional spatial soliton propagation in bulk Kerr material," *Opt. Lett.*, vol. 17, pp. 844–846, 1992.
[5] G. P. Agrawal, "Induced focusing of optical beams in self-defocusing nonlinear media," *Phys. Rev. Lett.*, vol. 64, pp. 2487–2490, 1990.
[6] A. Stenz, M. Kauranen, J. Maki, G. P. Agrawal, and R. Boyd, "Induced focusing and spatial wave breaking from cross-phase modulation in a self-defocusing medium," *Opt. Lett.*, vol. 17, pp. 19–24, 1992.
[7] J. Hickmann, A. Gomes, and C. De Araujo, "Spatial cross-phase modulation effects in a self-defocusing medium" in *Proc. IQEC'92*, paper ThC6, p. 358.
[8] S. Dinev, A. Dreischuh, and I. Ivanova, "Induced deflection of optical beams in an off-axis geometry," *J. Mod. Opt.*, vol. 39, pp. 667–671, 1992.
[9] M. Born and E. Wolf, *Principles of Optics*. Moscow: Nauka, 1976.
[10] A. Dreischuh, E. Eugenieva, and S. Dinev, "Pulse shaping and shortening by spatial windowing of induced-phase modulated probe wave," *IEEE J. Quantum Electron.*, vol. 30, pp. 1656–1661, 1994.
[11] I. Golub, "Beam deflection and ultrafast angular scanning by a time-varying optically induced prism," *Opt. Commun.*, vol. 94, pp. 143–146, 1992.
[12] O. Werner, B. Fischer, and A. Lewis, "Strong self-defocusing effect and four-wave mixing in bacteriorhodopsin films," *Opt. Lett.*, vol. 17, pp. 241–243, 1992.
[13] S. Durbin, S. Arakelian, and Y. Shen, *Opt. Lett.*, vol. 6, pp. 411–413, 1981.
[14] S. Dinev, A. Dreischuh, and I. Ivanova, "Spatio-temporal analysis of all-optical streaking," *Appl. Phys.*, vol. B-56, pp. 34–38, 1993.

**N. Goutev**, photograph and biography not available at the time of publication.

**A. Dreischuh**, photograph and biography not available at the time of publication.

**S. Baluschev**, photograph and biography not available at the time of publication.

**S. Dinev**, photograph and biography not available at the time of publication.